JOURNAL OF PROPULSION AND POWER
Vol. 29, No. 2, March–April 2013

Characterization of a Heaterless Hollow Cathode

V. Vekselman,* Ya. E. Krasik,† S. Gleizer,‡ and V. Tz. Gurovich§
Technion–Israel Institute of Technology, 32000 Haifa, Israel
and
A. Warshavsky¶ and L. Rabinovich**
Rafael Advanced Defense Systems Ltd., Ministry of Defense, 31021 Haifa, Israel

DOI: 10.2514/1.B34628

The parameters of a thermionic heaterless hollow cathode operating in the diode mode were determined using various diagnostic methods, and studied in relation to the discharge current, in the range 0.5–1.5 A, the orifice plate–anode gap, and the xenon-gas flow rate. It was shown that the cathode ignition consists of breakdown, heating, and keeping phases, and it realizes in the timescale of a few seconds depending on the xenon-gas flow rate. Dependencies of the cathode and orifice potential vs the gas flow rate and discharge current were obtained. The plasma plume parameters (plasma density and temperature) were studied using double Langmuir probe and spatial resolved optical spectroscopy. The energy distribution of the generated electron beam was obtained by the retarding energy analyzer and biased collimated Faraday cup. The processes involved in the hollow cathode ignition, heating, and dc operation are discussed, and the influence of initial conditions on the reliability and efficiency of the operation of a hollow cathode is determined. Finally, a simple model for estimation of the emitter temperature during the cathode operation is suggested.

I. Introduction

THE development of electron sources is of continuous interest due to their various applications, such as in high-power microwave generation [1,2], electron-beam welding [3], surface modifications [4], plasma propulsion [5], and so on. Electron emission from solid cathodes based on either thermionic emission [6] or field-electron-emission [7] phenomenon is routinely used to generate electron beams, and these electron sources satisfy many customer requirements. However, the constantly growing requirements of innovative applications, especially plasma propulsion [8,9], laser [10,11], and high-power microwave [12] generation, have increased the interest in the development of novel electron sources, with emphasis on specific properties, such as high emissivity, long lifetime, energy saving, reliability, and fast startup. Among these novel electron sources, the plasma source [13,14] can be considered a promising candidate. The operation of plasma sources is based on the extraction of electrons from the plasma boundary, which has high emissive properties (up to 100 A/cm^2), an arbitrary area, and sufficient homogeneity. These electron sources allow the formation of plasma of the preferred parameters, the most important of which are density and temperature, and with specified energy consumption in a suitable time interval.

To meet the requirements for microsatellite propulsion and satellite orbit control [8], it is preferable that the cathode ignition time be in the millisecond timescale so that the thruster can be turned on in a few seconds or less, be power effective, and that the cathode design be propellant saving, lightweight, and simple. In addition, general operating requirements for plasma-propulsion applications dictate that its components have a long lifetime and operate reliably. Conventional electron sources that are used in electric-propulsion systems are heater-based thermionic hollow cathodes [15,16]. This type of cathode requires an external heater to increase the temperature of the emitter sufficiently to achieve the necessary current density of thermionic electron emission from its surface [5]. These electrons ionize the residual gas inside the hollow cathode (HC) and form the plasma, serving as a source of electrons extracted from its boundary toward the anode. Continuous plasma formation is sustained by thermionic electron emission from the emitter, and extraction of electrons from the plasma leads to the appearance of the positive potential of the plasma with respect to the emitter. This results in ion emission from the plasma boundary toward the emitter and the acquisition of sufficient energy inside the plasma-emitter sheath for the cathode to operate in a self-heating mode. The duration of the startup procedure (i.e., when the cathode begins to operate in the self-heating mode and the external-heating power supply can be turned off) of such cathodes is typically hundreds of seconds [17], and the power consumption is considerable because the emitter is heated by an external heater. The lifetime of the conventional thermionic HC is determined mainly by two major effects: emitter-material poisoning and heater failure. Thus, to increase the reliability of the system and to avoid possible heater failure, a heaterless cathode design was proposed and implemented by Schatz, Arkhipov, Sarvey-Verhey and Hamley, Gallimore, Koroteev, and other researchers [18–22]. The proposed heaterless HC design and operational characteristics can still be improved upon to decrease the power consumption, increase the cathode lifetime, and make the startup procedure more reliable and the design more robust.

In the present paper, the experimental results of the characterization of the heaterless thermionic hollow cathode (HTHC) designed by the National Aerospace University–Kharkiv Aviation Institute (KhAI) [23] will be presented. This HTHC differs from the cathodes mentioned previously in its simpler design and lower power consumption, characteristics that expand its potential application in electric-propulsion systems, namely, in mid- and low-power Hall-effect thrusters to ignite the discharge and to neutralize the ion beam generating the thrust. Therefore, the understanding of the physical phenomena and parameters that govern the ignition and heating of the HTHC, and the initiation and the characteristics of the discharge becomes of prime importance. These features of the HTHC were studied in the present research study to gain a better insight into the physical processes during the cathode operation. In particular, the HTHC ignition behavior, the initiation of the main discharge, and plasma parameters were determined under various initial conditions.

Received 26 March 2012; revision received 13 August 2012; accepted for publication 19 September 2012; published online 13 February 2013.

*Postdoctoral Fellow, Physics Department.
†Professor, Physics Department.
‡Senior Research Scientist, Physics Department.
§Senior Research Scientist, Physics Department.
¶Electric Propulsion System Engineer, P.O. Box 2250.
**Project Manager, P.O. Box 2250.

II. Experimental Setup

A scheme of the experimental setup, including some of the applied diagnostics, is shown in Fig. 1. A 1.8 m^3 stainless-steel vacuum chamber was pumped using a cryogenic pump (Austin Scientific M350) providing a background pressure below 1 mPa during experiments with the HTHC. The pressure was monitored using an Edwards ATC-E active thermocouple and an AIM-X active inverted magnetron gauge. An RGA-300 residual-gas analyzer was used to control the partial pressure of the residual gas in the vacuum chamber during the pumping and cathode operation. The xenon (Xe)-gas flow rate was controlled by an Alicat ALIMC-5SCCM mass flow controller calibrated for Xe in the range 0–5 sccm. (The unit sccm denotes standard cubic centimeter per minute.) The power system consists of a 30 V, 30 A Digimess power supply, an ignition block (IB) developed by KhAI for HTHC ignition, and a power supply TDK Lambda (600 V, 4 A) to sustain the main discharge between the emitter and the anode.

The voltage and current (see Fig. 2 for the electrical scheme of the experimental setup) were monitored during HTHC ignition and its operation in the diode mode using the National Instruments multifunction data-acquisition devices NI PCI-6133(14 bit, 2.5 MS/s/ch, simultaneous sampling) and NI USB-6218 (16 bit, 250 kS/s, isolated), respectively. The NI USB-6218 with additional isolated operational amplifiers and power suppliers (up to ± 200 V) was also used to control the diagnostic system and voltage measurements (see Fig. 1). A personal computer was used for data acquisition and to control the components of the experimental setup (power supplies, mass flow controller, RGA, etc.) using the LabVIEW code.

An artist's rendering of the HTHC is shown in Fig. 3. The emitter of the HTHC is made of W matrix impregnated with $Ba_3Sr_4O_9$ [24]; its internal diameter is 0.4 mm and length is 2 mm. The emitter is placed inside a thin Mo tube. The distance between the emitter and the orifice is ~2 mm. To maintain the high temperature of the emitter, an intermediate-screening coaxial electrode (shielding) is used. The external diameter of the HTHC is 8.5 mm, and the total length and mass are 80 mm and 33 g, respectively.

The plasma in the orifice plate–anode region was studied using various electrical probes [double Langmuir probe, retarding energy analyzer (REA), and collimated Faraday cup (CFC)] and a non-disturbing spectroscopic technique. The Xe-gas-density distribution in relation to the distance from the orifice toward the anode was studied using a calibrated Penning probe. The plasma density and electron temperature inside the orifice plate–anode gap were studied using a double Langmuir probe [25,26], which consists of two W wires, each 0.5 mm in diameter and 5 mm in length; the distance between the wires is 1 mm. The probe was aligned perpendicular to the cylindrical cathode axis and could be moved along the HTHC and/or probe axes. The energy spectrum of electrons was obtained using a biased CFC and REA, placed behind the anode, which was made of stainless-steel plate 2 mm in thick and having 1 mm in diameter central hole (see Fig. 1). The application of the REA and CFC allows one to obtain the deviation of the plasma electron-energy distribution function (EEDF) from equilibrium distribution. In addition, the EEDF gives some predictions of voltage drops inside the sheath formed in plasma discharge, thus predicting the ion flux toward the emitter and the orifice plate, which is a crucial issue for estimating the erosion of these parts.

The optical images of the plasma light emission were captured by a fast-framing intensified camera, 4QuikE. A spectroscopic research of the plasma parameters was carried out using an optical system (Nikon 70–300 mm objective) installed to guide the emission from the plasma to the imaging spectrograph (Chromex 500is) coupled with the 4QuikE camera (Fig. 1). The spectral resolution was 0.05 nm/pix (pixel is square, 8.62×8.62 μm) with a 50 μm entrance slit. The spectral sensitivity and absolute intensity of the system were calibrated using an Oriel standard irradiance lamp (SN7-1732).

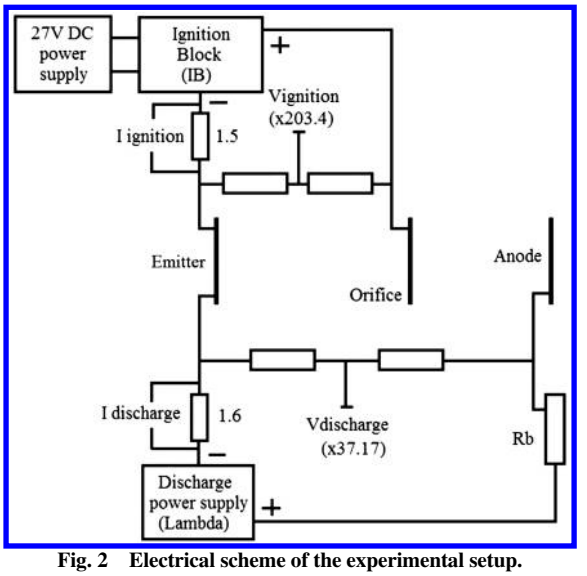

Fig. 2 Electrical scheme of the experimental setup.

III. Experimental Results

A. Cathode Ignition

The HTHC was introduced to reduce the cathode complexity, to decrease the duration of the cathode heating and the start time of the Hall-effect thruster, and to increase the reliability of the thruster's operation. The main idea in the HTHC operation is that the emitter is rapidly heated by the ions emitted from the plasma, which is ignited by the arc discharge between the emitter and the orifice using a pulsed generator incorporated in the IB. Thus, it is important to study the breakdown of the emitter–orifice (EO) plate gap, plasma formation, and the filling of the hollow emitter. Note here that HTHC ignition means the ability of the emitter to provide enough thermionic electrons to initiate and sustain the main discharge between the

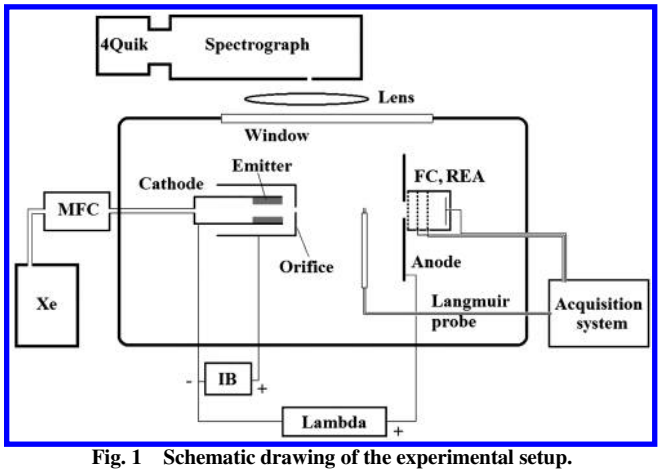

Fig. 1 Schematic drawing of the experimental setup.

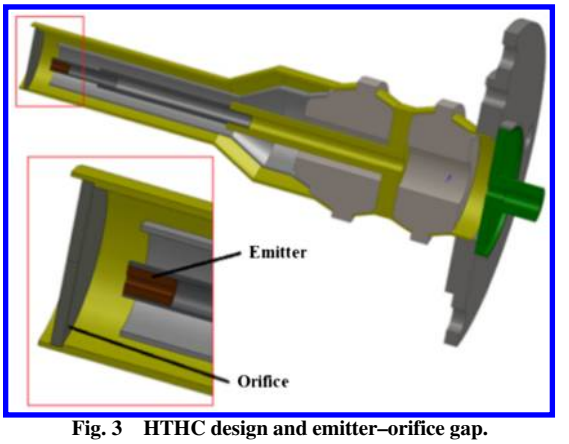

Fig. 3 HTHC design and emitter–orifice gap.

emitter and the anode. In the case of an HTHC, this is equivalent to establishing a low-voltage, but relatively high-current plasma discharge between the emitter and the orifice. This plasma penetrates the orifice and starts to serve as the source of electrons, which are accelerated toward the anode, producing ionization of the gas inside the orifice plate–anode gap. Simultaneously, this plasma fills the hollow emitter's inner volume and acquires a positive potential with respect to the emitter, ensuring that the emitter is heated at the necessary rate by ions emitted from the plasma boundary toward the emitter.

The HTHC ignition tests were carried out using the SHC-M1 flight-model cathode [23] and the cathode (hereafter, this cathode will be denoted as the test cathode) that has the same emitter and dimensions as the SHC-M1 flight model, except for the keeper and shielding. Namely, this test cathode was placed inside the quartz tube, and the shielding was removed to allow optical access to the EO-plate gap (see Fig. 4). The O-ring-based connections between the quartz tube and the orifice plate, and the quartz tube and the gas distributor result in relatively high Xe leakage, which was compensated by a higher Xe flow rate to keep the same conditions (pressure) inside the test cathode. The absence of a coaxial electrode, which is commonly used in HC for shielding of the emitter radiation, increases the radiation losses with the increase in the emitter temperature. Therefore, this test cathode was used only to study the ignition process; the operation time of the test cathode was reduced to a few minutes. Thus, one can consider that quantitatively, the laboratory test cathode and flight-model cathode could operate slightly differently, but the ignition of these cathodes should be similar.

The studies of the test-cathode ignition were carried out in the diode mode (Fig. 1) inside the vacuum chamber, where the vacuum was kept at 8×10^{-4} Pa (without Xe-gas feeding). The gap between the test-cathode emitter and the orifice plate was varied in the range of 1–3 mm. In this set of experiments, the time delay between the sequential ignitions of the test cathode was kept at ~5 min, while maintaining the propellant flow to attain the same initial conditions for ignition. To collect statistics, at least 20 ignitions were performed at each operating point.

Typical volt–ampere characteristics of the test-cathode ignition and the development of the main discharge between the emitter and the anode (see Fig. 2) are shown in Fig. 5. It can be seen that the ignition process can be divided into three phases: 1) breakdown, 2) heating, and 3) keeping.

The first breakdown phase is characterized by a fast decrease in the amplitude of the high-voltage pulse applied between the emitter and the orifice, and formation of the plasma inside the EO gap (see also Fig. 6a). This phase occurs in the millisecond timescale, and the breakdown voltage threshold V_{br} depends on the initial conditions

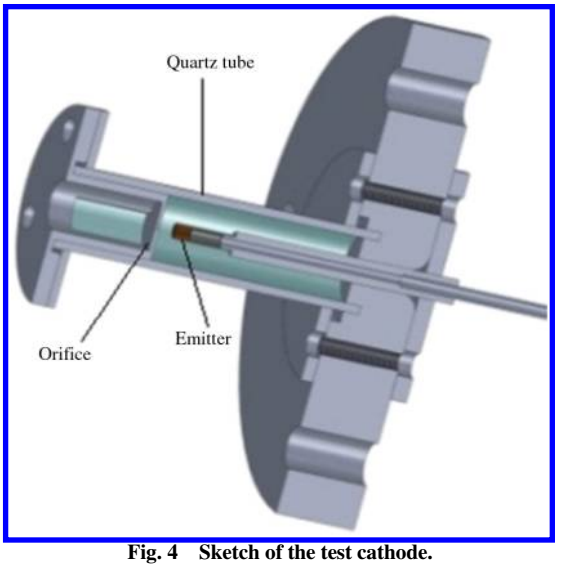

Fig. 4 Sketch of the test cathode.

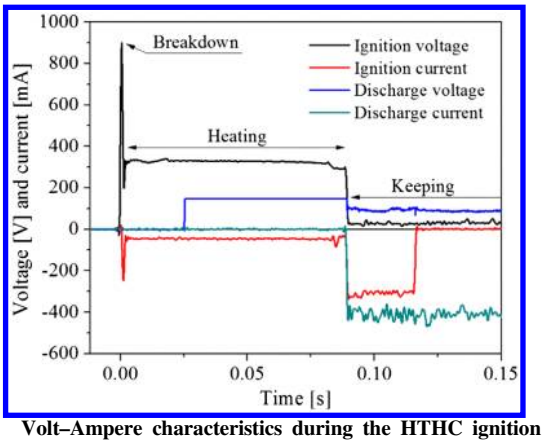

Fig. 5 Volt–Ampere characteristics during the HTHC ignition and discharge development. The anode–orifice plate gap is 3 cm; the Xe gas flow rate is 1 sccm.

(i.e., the value of the Xe-gas pressure p and the EO gap d_{e-o}, and qualitatively agrees with Paschen's law [27,28].

The second phase of the cathode ignition is characterized by an almost constant voltage drop of ~300 V, with a current of ~40 mA between the emitter and the orifice plate. These parameters are determined by the electrical scheme of the IB to avoid a high-current-density-arc mode with a current of up to 3 A, which is typical for the breakdown phase. (It cannot be resolved in Fig. 5 because of the millisecond-timescale duration of the breakdown phase.) This so-called heating phase is necessary to obtain sufficient heating of the emitter by the ions that are emitted by the plasma and accelerated inside the sheath between the plasma and the emitter. Also, it is supposed that during this phase, the plasma formation occurs inside the entire volume of the emitter due to initial plasma expansion and additional plasma formation caused by the ionization of the Xe gas by thermionically emitted electrons.

The last, third keeping phase is characterized by the low-voltage (~30 V) and high-current (~300 mA) mode of the discharge between the emitter and the orifice plate. In this phase, the emitter is heated and provides thermionic current that is limited by the IB. The duration of this phase is generally unlimited, and the development of the main discharge (emitter–anode) allows the IB to be switched off.

An optical observation of the EO gap during the test-cathode ignition showed different forms of gas discharges. Typical frames (frame duration of 1 μs) of the plasma luminosity obtained during these phases at different times (see Fig. 5) are shown in Fig. 6.

One can see that almost immediately after the termination of the breakdown phase (beginning of the heating phase), the discharge has a well-defined form with some inclination with respect to the symmetry axis (see Fig. 6a). One can assume that this discharge inclination occurs because the EO-gap breakdown happens between the nonuniformities that are arbitrarily located at the edges of the emitter tube and the orifice-plate surface. Later in the heating phase, one obtains redistributions of the discharge-channel luminosity, which becomes almost axial symmetrical with the spreading of the discharge channel toward the orifice plate (see Fig. 6b). At the end of the heating phase, the luminosity of the discharge channel decreases, becoming diffuse with an increase in the plasma channel's diameter, especially in the vicinity of the orifice plate (see Fig. 6c). Finally, an increase in the thermionically emitted current from the heated emitter

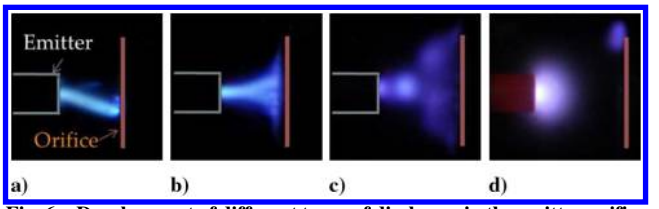

Fig. 6 Development of different types of discharge in the emitter-orifice plate (EO) gap during the emitter heating. The EO gap is 1.9 mm; the Xe flow rate is 1 sccm.

leads to the generation of a denser plasma inside the hollow emitter and transition to the last [i.e., keeping phase (see Figs. 5 and 6d)]. Note that this keeping phase is realized regardless of the main discharge voltage applied between the emitter and the anode using the other power supply (see Fig. 2). Thus, to conclude, the appearance of the keeping phase manifests the ignition of the HTHC.

The change in the form and luminosity of the discharge channel is related to the plasma's radial expansion and penetration into the emitter inner volume. The latter leads to the heating of the emitter by the plasma ions, allowing the emitter to become the prime source of current-carrying electrons. These electrons can uniformly ionize the Xe gas inside the emitter and in the EO gap. The almost-conical expansion of the discharge channel toward the orifice plate can be related to the larger pressure inside the emitter and the expansion of the gas flow toward the orifice plate. Also, the conical structure of the plasma-discharge channel can be related to the divergence of the electrons when these electrons are emitted from the pointlike source (i.e., from the plasma boundary in the vicinity of the emitter).

The application of the main discharge voltage ($\lesssim$300 V) between the emitter and the anode during the heating phase, when the potential of the orifice plate could be as high as ~300 V with respect to the emitter, does not lead to the simultaneous turn-on of the main discharge. Here, note that when the main discharge voltage is applied during the keeping phase, the development of the main discharge occurs almost simultaneously (i.e., within several tens of milliseconds) due to the potential distribution gradually increasing downstream toward the anode. Thus, the necessary condition for the reliable development of the main discharge with a current of several hundreds of milliamperes between the emitter and the anode is the drop in the voltage inside the EO gap down to several tens of volts that is realized when the keeping phase has been established.

In addition, it was found that during the heating phase, for a Xe-gas mass flow rate G in the range $(1 - 1.5)$ sccm, one obtains a diffuse and satisfactory uniform-glow-type discharge between the emitter and the orifice plate characterized by a voltage drop of 200–300 V and an effective and homogeneous heating of the emitter. At larger values of G (i.e., $G > 1.5$ sccm), an arc formation was realized after the breakdown of the EO gap with slower and visible nonuniform heating of the emitter. In this case, one obtains a drop in the orifice-plate potential down to ~50 V, allowing one to achieve ignition of the main emitter–anode discharge almost simultaneously with the termination of the breakdown phase, even at the time when the emitter is still cold and cannot supply thermionically emitted electrons. Note that in this ignition mode, the main discharge current starts from lower values and increases to a nominal current value with the heating of the emitter. Thus, one can conclude that the ignition of the main discharge is occasioned by the electrons extracted from the boundary of the arc plasma that penetrates the orifice.

The turnoff of the IB terminates the current flow in the EO-plate circuit, and the orifice plate begins to float (see Figs. 2 and 5). At that time, the main discharge current and the voltage drop between the emitter and the anode were varied in the ranges 0.5–1.5 A and 60–120 V, respectively. Here, note that a fast increase in the density of the electrons extracted from the plasma at the beginning of the main discharge could lead to an increase in the plasma positive potential [29] and, respectively, to an increase in the energy of the ions and in the ion current density toward the emitter.

B. HTHC Operation in Diode Mode

A typical luminosity of the plasma inside the orifice plate–anode gap of the HTHC (SHC-M1) running in the diode mode is shown in Fig. 7.

One can see a rather sharp boundary between the plasma plume, which emits intense light at the exit of the orifice, and the diffuse plasma, with significantly less light emission in the remaining orifice plate–anode gap. Such nonuniform light-emission distribution in the orifice–anode gap indicates also plasma density and temperature gradients. For instance, the plasma plume can be considered to obtain a potential close to the emitter potential and to play the role of the source of electrons emitted from its boundary toward the anode,

Fig. 7 HTHC (SHC-M1) running in diode mode. The discharge current is 0.9 A, the Xe-gas flow is 1.5 sccm, and the orifice plate–anode gap is 2 cm.

producing gas ionization inside the orifice plate–anode gap. The larger plasma density in the plume can be related to the larger density of neutrals in the vicinity of the orifice and, respectively, to a faster ionization rate at that location.

The volt–ampere dependencies of the HTHC reveal its nonlinear behavior in relation to the Xe-gas flow rate (see Fig. 8). For instance, when the flow rate is $\lesssim$1 sccm, one obtains a negative slope in the volt–ampere dependence showing the decrease in the diode impedance, $Z_d \sim 1/I_d$, in which I_d is the discharge current flowing between the emitter and the anode. However, a further increase in the gas flow rate leads to a positive slope of the volt–ampere dependence. In addition, measurements of the voltage drop between the EO plate φ_{e-o} allow one to obtain the dependencies of φ_{e-o} and the voltage drop between the orifice plate and the anode φ_{o-a} in relation to the value of the main discharge current shown in Fig. 9. One can see that for both Xe-gas flow rates, the value of φ_{e-o} gradually decreases, whereas φ_{o-a} tends to increase with an increase in the value of I_d. Note also a sharp increase in φ_{o-a} at $I_d \geq 0.9$ A for a gas flow rate of 1 sccm, and that for lower flow rates, the increase in the main discharge voltage starts at a lower discharge-current value.

To explain qualitatively the obtained decrease in the potential difference φ_{e-o} between the EO plate and the discharge current, consider the dependence of φ_{e-o} on the plasma electron temperature. Indeed, the discharge current flowing through the dense and collisional plasma inside the emitter and in the space between the EO plate is proportional to the electron temperature T_e. Namely, assuming uniform cross-sectional current-density distribution, the discharge current is $I_d \approx n_e e V_d S_o$, in which S_o is the cross-sectional area of the plasma approximately equal to the cross-sectional area of the emitter hole, e is the electronic charge, and n_e is the plasma electron density. The rate of the plasma production can be expressed as $\mathrm{d}ne/\mathrm{d}t = n_a n_e \langle \sigma_i v_{\mathrm{th}} \rangle - n_i c_s S - n_e^2 k$, in which n_a, n_e, and $n_i = n_e$ are the atom, electron, and ion densities, respectively; $v_{\mathrm{th}} =$

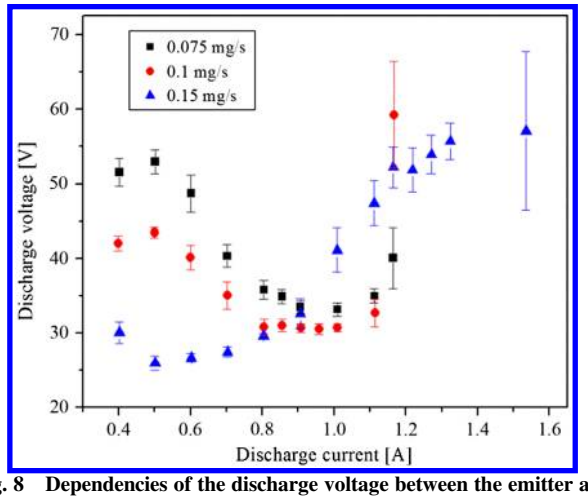

Fig. 8 Dependencies of the discharge voltage between the emitter and the anode, and the current for different Xe-gas flow rates. The orifice plate–anode gap is 2 cm.

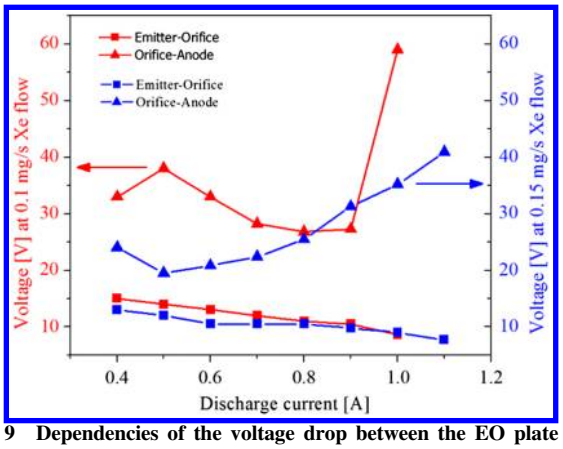

Fig. 9 Dependencies of the voltage drop between the EO plate and orifice plate-anode versus the discharge current. The orifice plate-anode gap is 2 cm.

$\sqrt{kBTe/me}$ is the electron thermal velocity; σ_i is the ionization cross section; $c_s = \sqrt{kBTe/Mi}$ is the sound velocity of ions; S is the area of plasma surface; and k is the recombination coefficient. In the steady-state mode of the HC operation, one obtains $\mathrm{d}ne/\mathrm{d}t = 0$, which results in

$$n_e = \frac{\sqrt{k_B T_e}}{k}\left(n_a\left\langle\frac{\sigma_i}{\sqrt{m_e}}\right\rangle - \frac{S}{\sqrt{M_i}}\right) \propto \sqrt{T_e}$$

Thus, the drift velocity of the current-carrying electrons, $v_d \approx v_{\mathrm{th}}(4m_e/M_i)^{1/2} \approx 1.7\times10^5(T_e)^{1/2}$, in which M_i is the Xe-ion mass. Thus, one can see that the discharge current is $\propto T_e$.

Now, consider the value of $\varphi_{e-o} = \varphi_{e-\mathrm{pl}} + \varphi_{\mathrm{pl}} - \varphi_{\mathrm{pl}-o}$, in which $\varphi_{e-\mathrm{pl}}$ is the cathode fall between the emitter and the plasma, φ_{pl} is the potential drop in the plasma because of its finite resistivity, and $\varphi_{\mathrm{pl}-o}$ is the negative potential drop inside the sheath between the plasma and the floating orifice plate. The value of $\varphi_{\mathrm{pl}-o}$ can be estimated using plasma electron temperature, and assuming the equality of electron and ion currents toward the floating orifice plate as $\varphi_{\mathrm{pl}-o} \propto AT_e$, in which $A = (2k_B/e)\ln(M_i/m_e)$ is the coefficient. The potential drop along the plasma channel is $\varphi_{\mathrm{pl}} = I_d R$, in which R is the plasma channel resistance, which can be estimated as $R = \eta l_{\mathrm{pl}} S_{\mathrm{pl}}^{-1}$. Here, $\eta \approx 5\times10^{-2}T_e^{-3/2}$ is the specific resistivity of the plasma [30], and l_{pl} and S_{pl} are the length and cross-sectional area of the plasma channel, respectively. Thus, the potential drop along the plasma channel is $\varphi_{\mathrm{pl}} \propto B\cdot T_e^{-1/2}$, in which $B = f(S_{\mathrm{pl}}, l_{\mathrm{pl}})$. One can assume that in the dc mode of the HTHC operation, the value of $\varphi_{e-\mathrm{pl}}$ depends rather little on the plasma electron temperature. Indeed, one can suggest that an increase in the value of I_d leads to a short-duration transition period. During this period, first, one obtains an increase in $\varphi_{e-\mathrm{pl}}$ because of a larger electron current being extracted from the plasma boundary in the vicinity of the orifice output toward the anode [29]. This leads to a larger energy being delivered to the emitter by the ion flow and additional heating of the emitter. The latter dictates the increased thermionically emitted current density and energy of electrons entering into the plasma and, respectively, the increase in the plasma density due to the additional ionization of neutrals by the increased flux of emitted electrons. The increased density of the plasma leads to an increase in the ion flux toward the emitter, which allows a decrease in $\varphi_{e-\mathrm{pl}}$, keeping the same ion energy density flow toward the emitter. Thus, one can consider that $\varphi_{e-o} \propto \mathrm{const} + B\cdot T_e^{-1/2} - AT_e$ and, respectively, $(d\varphi_{e-o}/\mathrm{d}T_e) \propto -1/2(B\cdot T_e^{-3/2}) - A < 0$ (i.e., an increase in the plasma temperature, which is proportional to I_d) lead to a decrease in the potential drop between the emitter and the orifice plate. This qualitative analysis of the orifice-plate potential does not take into account the flux of ions from the plasma formed in the orifice plate–anode gap toward the orifice, which also depends on the value of I_d. In fact, as will be shown in Sec. III.C, an increase in the value of I_d leads to an increase in the plasma density in the orifice plate–anode gap and, respectively, to an increase in the ion flux toward the orifice, thus increasing its potential.

One can now make a rough estimate of the minimum plasma density inside the orifice required to carry the discharge current. The current density can be estimated as ~4 kA/cm^2 for a value of $I_d \sim 0.7$ A. Here, a uniform cross-sectional current-density distribution, $j_e \approx I_d/S_{\mathrm{or}}$, was assumed, in which $S_{\mathrm{or}} \approx 1.8\times10^{-4}$ cm^2 is the cross-sectional area of the orifice. In the case of collisional plasma, the drift velocity of the current-carrying electrons can be estimated as $\sim2\times10^5$ cm/s for $T_e \sim 1$ eV. Thus, one obtains that the minimal plasma density $n_e \approx j_e/eV_d \sim 1.47\times10^{17}$ cm^{-3} inside the orifice. This plasma is characterized by electron–ion collisions having a frequency $\nu_{\mathrm{ei}} = 2\times10^{-6}n_eT_e^{-3/2}\ln\Lambda \approx 1.4\times10^{12}\mathrm{s}^{-1}$, in which $\ln\Lambda \approx 10$ is the Coulomb logarithm. Now, one can estimate a mean free path of the plasma electron as $\lambda_e \le V_{\mathrm{th}}/\nu_{\mathrm{ei}} \approx 1\mu$m, validating the assumption that the plasma is highly collisional. The resistance $R_{\mathrm{or}} = \eta l_{\mathrm{or}} S_{\mathrm{or}}^{-1}$ of the plasma inside the orifice, in which $l_{\mathrm{or}} = 5\times10^{-2}$ cm is the length of the orifice, with an ionization degree larger than 1%, is determined by the electron–ion collisions and almost does not depend on the plasma density [30]. Thus, for $T_e \approx 1$ eV (0.7 A), one obtains the resistivity of the plasma inside the orifice $R \approx 14\ \Omega$ and the potential drop $\Delta\varphi_{\mathrm{or}} \le 10$ V along the plasma channel within the orifice.

It may be supposed that the potential drops along the discharge plasma channel inside the emitter, and the EO could be similar or smaller because of the significantly larger cross-sectional areas of the plasma. (The distribution of potential inside of the conventional HC was measured by Goebel et al. [31] and Jameson et al. [32].) Thus, these estimates showed that the main potential drop between the emitter and the anode, which is ~50 and ~70 V for $I_d = 0.4$ A and $I_d = 1.1$ A, respectively, occurs in the plasma sheaths that could develop inside the orifice, in the vicinity of the emitter, and between the orifice plasma and the anode. Here, note that the sharp increase in the potential drop between the orifice plate–anode that was obtained in the case of a smaller value of $G = 1$ sccm and at $I_d > 0.9$ A could be related to the formation of a double sheath inside the orifice-plasma channel with a potential drop, allowing current continuity in the case of insignificant plasma density.

Now, analyze qualitatively the negative slope of volt–ampere dependence obtained for voltage difference between the emitter and the orifice (see Fig. 9). In general, an increase in the value of I_d requires a larger emitter temperature, which is determined only by an ion energy flux toward the emitter from the plasma. Namely, the increase in the emitter temperature can be achieved either due to an increase in the ions' energy, which assumes an increase in the potential difference in the plasma–emitter sheath, or by an increase in the density and temperature of the plasma allowing a larger flux of ions to be emitted without a change in potential difference. As already discussed, an increase in the potential difference leads to a larger amount of energy being delivered to the emitter by the ion flow and an increase in the emitter temperature. The latter increases the emitted electron current density and energy of electrons, which increases the plasma density due to the increased ionization rate of neutrals. The increased density and temperature of the plasma cause an increase in the ion flux toward the emitter, allowing a decrease in the potential difference in the plasma–emitter sheath, keeping the required ion energy density flow toward the emitter. It is understood that careful numerical modeling is required because the processes discussed previously are nonlinear processes.

C. Langmuir-Probe Measurements

Using a double Langmuir probe, the plasma density and electron temperature were obtained [30] at different distances from the output of the orifice plate and for different values of I_d. The obtained dependencies of $n_e = f(I_d)$ at distances $z = 1$ cm and $z = 2$ cm along the symmetry axis for $G = 1$ sccm and $G = 1.5$ sccm are shown in Fig. 10.

One can see that the plasma density inside the orifice plate–anode gap is $\le 5\times10^{10}$ cm^{-3} at the symmetry axis within the studied range of the discharge current. In addition, it was found that the plasma

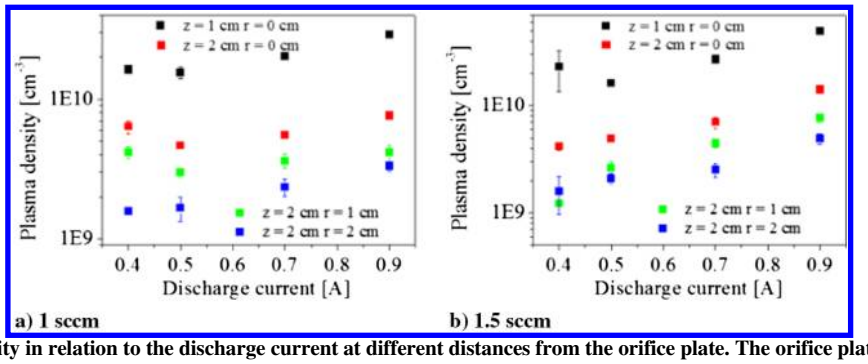

Fig. 10 Plasma density in relation to the discharge current at different distances from the orifice plate. The orifice plate–anode gap is 3 cm.

density already decreases ~10 times at radius $r = 2$ cm. Note that the distance $z = 1$ cm is the distance where the light intensity of the dense plasma plume that is formed at the exit of the orifice is terminated (see Fig. 7). Thus, the entire orifice–anode gap is filled by dilute plasma with a screening length ≥ 0.1 mm. One can explain the formation of this plasma as resulting from the Xe-gas ionization by electrons emitted from the boundary of the dense plasma plume. Indeed, the propagation of the electron beam with a current density of $\sim(2\text{–}5)\text{A/cm}^2$ and energy of a few tens of electron volts requires background ions with a density $\sim(1\text{–}2) \times 10^{10}$ cm^{-3}.

When $G = 1$ sccm, one can see a gradual increase in the value of n_e with the increase in I_d, except in the case of $I_d = 0.4$ A, in which the value of n_e is slightly larger than for $I_d = 0.5$ A. This can be explained by a larger electron temperature at a low value of I_d [see Fig. 11a where the dependence $T_e = f(I_d)$ is shown]. Indeed, in the case of larger electron energy, one can obtain an increase in the ionization rate even for a smaller electron density because the ionization rate $\mathrm{d}n_i/\mathrm{d}t = n_e n_{Xe}\langle\sigma_i V_{\mathrm{th}}\rangle$, in which n_{Xe} is the Xe neutral-atom density and σ_i is the impact-ionization cross section depending on the plasma electron energy.

A further increase in the discharge current above $I_d = 0.5$ A leads to a gradual increase in the plasma density, which agrees also with the electron-temperature dependence in this range of I_d (Fig. 11a). Along the symmetry axis, the plasma density was found to decrease almost linearly (i.e., at distances of 1 and 2 cm from the orifice plate, the density decreases by ~1.8 times). When $G = 1.5$ sccm (see Fig. 11b), one obtains a gradual increase in the value of T_e vs I_d, indicating that, due to the increased gas flow rate, the plasma parameters inside the emitter are changed in self-consistent mode to provide the desired discharge current without increasing the value of T_e at $I_d < 0.5$ A. This can be explained by the increased density of neutrals, which allows an increased ionization rate and plasma density without an increase in the plasma potential with respect to the emitter wall. The latter leads to sufficient ion flux toward the emitter to maintain its temperature to emit the desired electron current density.

D. Retarding Energy Analyzer and Faraday Cup

A typical EEDF obtained using the biased CFC is shown in Fig. 12. The design of the Faraday cup includes a grid placed in front of the collector. The grid was used to decrease the density of the plasma inside the CFC. A variable negative biased potential φ_b was applied to the collector of the CFC with respect to the CFC screen box and grid. Thus, only the electrons having energy E_e larger than $|e\varphi_b|$ can be registered by the collector together with plasma ions. The derivative of the collector current vs the collector-bias voltage provides an energy distribution function of electrons.

One can see that the EEDF consists of two Gaussian-like maxima at a collector bias of 0 and 22 V, respectively. The first peak is broadened by ~5 eV and reflects the plasma electron temperature, whereas the second energetic peak indicates the presence of an electron beam. A similar EEDF was obtained in [33] for conventional thermionic HC. The EEDFs obtained using the REA are shown in Fig. 13. These data show similar results, namely, energetic electrons have maximum in the energy spectra in the range 10–35 eV (see Fig. 13a) depending on the value of I_d. One can see that an increase in the discharge current leads to an increase in the maximum of the EEDF; an increase in the gas flow rate decreases this value (see Fig. 13b).

The obtained EEDF cannot be used to determine the location(s) where electrons gain energy larger than the thermal energy of plasma electrons. In fact, one can consider several locations where electrons acquire directed energy, namely, the emitter–plasma sheath, the double sheath inside the orifice (in the case of insignificant plasma density), the dense plasma plume–dilute plasma sheath, and the sheath between the dilute plasma and anode. The obtained spreading in the EEDF indicates that electron acceleration does not occur only in the plasma–anode sheath. Also, it is not likely that thermionically emitted electrons accelerated inside the emitter–plasma sheath or electrons accelerated in the double sheath, which could be formed inside the orifice, can contribute to the obtained energetic electrons because of energy losses and fast electron thermalization in the dense plasma existing inside the emitter and the orifice. Thus, one can suppose that the main electron acceleration occurs inside the sheath formed between the dense plasma plume and the dilute plasma formed in the vicinity of the orifice-plate output. It is understood that additional nondisturbing diagnostics should be applied to determine the location of these sheaths and their potential distribution inside the orifice plate–anode gap.

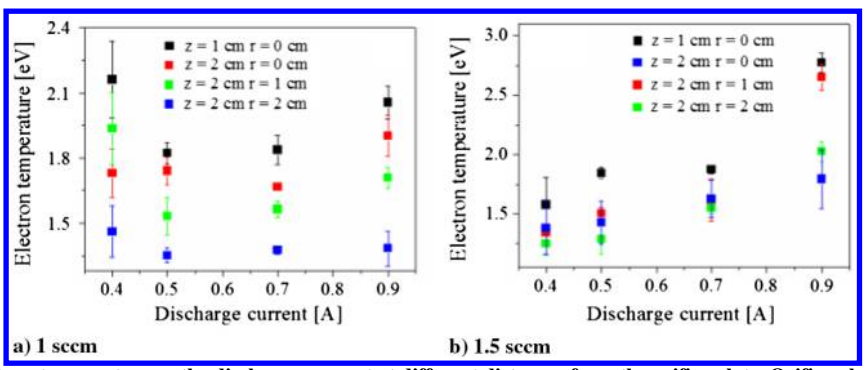

Fig. 11 Plasma electron temperature vs the discharge current at different distances from the orifice plate. Orifice plate–anode gap is 3 cm.

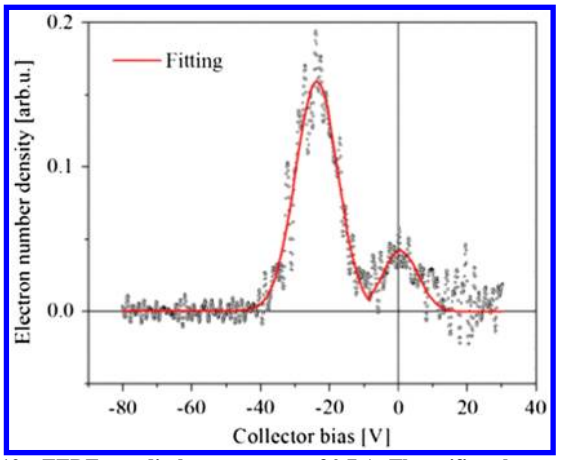

Fig. 12 EEDF at a discharge current of 0.7 A. The orifice plate–anode gap is 3 cm, and the Xe-gas flow rate is 1 sccm; arb.u. denotes arbitrary units.

E. Density of Xe Neutrals

The Xe-gas pressure P_0 in the gas-feedthrough system upstream the emitter (after the mass flow controller) was measured using a capsule dial gauge Edwards CG16K (range 0–100 torr) and presented in Fig. 14a. For the cold emitter (at room temperature), the results were 2.13 and 2.62 kPa for the Xe-gas flow rates of 1 and 1.5 sccm, respectively. A significant increase in the Xe-gas pressure P_0', which was dependent on the discharge-current amplitude, was observed by this gauge during the HTHC operation in the diode mode (see Fig. 14b). One can see that an increase in the discharge-current amplitude leads to the increase in the gas pressure. Namely, at the Xe-gas flow rates of 1 and 1.5 sccm, an increase in the discharge current from 0.5 to 1.4 A leads to the increase in pressure in 1.4 and 1.2 times, respectively.

This significant increase in the gas pressure can be associated with plasma-window phenomenon [34,35], which allows one to maintain high gas-pressure gradients due to the high temperature of the plasma. In fact, there are two locations of hot plasma formation, namely, the inner emitter volume and the orifice channel, which can contribute to the obtained increase in the gas pressure during the HTHC operation.

First, consider the gas flow inside the emitter assuming that the temperature of neutrals is less or equals the emitter temperature $T_{\rm em}$. The equation of momentum conservation is $P_{\rm em}^{\rm out} - P_{\rm em}^{\rm in} = \rho v^2$, in which ρ is the density of the gas, v is the flow velocity, and $P_{\rm em}^{\rm in}$ and $P_{\rm em}^{\rm out}$ are the values of pressure in the upstream and downstream regions with respect to the emitter, respectively. The gas flow velocity can be expressed in terms of the mass flow rate of the gas G, as $v = G/\rho S$. The density of the gas can be written as $\rho = P_{\rm em}^{\rm in}\mu/kBT$em, in which k_B is the Boltzmann constant, and μ is the mass of a Xe atom. Thus, one obtains

$$P_{\rm em}^{\rm out} - P_{\rm em}^{\rm in} = \rho\frac{G^2}{\rho^2 S^2} = \frac{G^2}{S^2}\frac{kT_{\rm em}}{\mu P_{\rm in}}$$

or

$$(P_{\rm em}^{\rm in})^2 - P_{\rm em}^{\rm out}P_{\rm em}^{\rm in} + \frac{k_B T_{\rm em} G^2}{\mu S^2} = 0 \qquad (1)$$

Using a known value of the pressure at the input to the emitter and its cross-sectional area, $S_{\rm em} \approx 1.3\times10^{-7}$ m^2 one obtains $P_{\rm em}^{\rm out} \approx P_{\rm em}^{\rm in}$ for the emitter's temperature in the range 700–2000 K. Thus, the pressure at the orifice entrance is $P_{\rm or}^{\rm in} = P_{\rm em}^{\rm out} \approx P_{\rm em}^{\rm in}$. Now, using the measured pressure, $P_{\rm em}^{\rm in} = 3275$ Pa (for a discharge current of 0.5 A), the gas density $\rho_{\rm em} = P_{\rm em}^{\rm in}(\mu/k_B T_{\rm em})$ and the gas flow velocity $V_{\rm em} = G/S_{\rm em}\rho_{\rm em}$ can be estimated as $0.07 - 0.03$ kg/m^3 and 11–31 m/s, respectively, for the same gas temperature range 700–2000 K. One can see that the estimated gas velocity is significantly less than the gas sound velocity $C_S = \sqrt{\gamma P_0/\rho_0}$ (C_s = 273–462 m/s, respectively), which allows one to consider laminar gas flow.

In the case of the orifice, Eq. (1) can be used to estimate the value of critical temperature $T_{\rm cr} = (P_{\rm em}^2\mu S_{\rm or}^2)/(4k_B G^2) \cong 1300$ K above which the real roots of the equation do not exist. Here, $S_{\rm or}$ is the cross-sectional area of orifice, $S_{\rm or} \approx 1.8\times10^{-8}$ m^2 The physical meaning of the critical temperature is straightforward — above such temperature, the steady-state gas flow inside the orifice does not exist.

There is another method to estimate an average temperature inside the orifice using the data concerning the increase in the gas pressure together with a constant gas-mass flow rate. Consider the following model for a discharge current of 0.5 A and a gas mass flow rate of $G \approx 10^{-7}$ kg/s. A gas with pressure P_0 and density ρ_0 at normal temperature T_0 flows from a cylindrical tube with a cross-sectional area, $S_0 \approx 3\times10^{-6}$ m^2, into the orifice with less cross-sectional area, $S_{\rm or} \approx 1.8\times10^{-8}$ m^2, and the ratio, $\alpha = S_{\rm or}/S_0 \approx 5.6\times10^{-3}$. For the constant gas mass flow rate, one can write that $G = \rho_i V_i S_i$, in which V_i is the velocity of the gas in the tube and the orifice (indices $i = 0, 1$ correspond to the tube and the orifice, respectively). The temperature of the gas flowing through the orifice is significantly larger than the temperature of the gas in the tube due to the plasma formation inside the HTHC. This plasma heats the gas atoms due to collision and charge-exchange processes, leading to almost equal temperature between ions and neutrals. Therefore, to keep G = const, the value of the pressure in the input tube, 0, increases to a value $P_0' > P_0$.

First, consider the case of cold-gas flow. In the experiment, it was measured that in the input tube 0 in the case $G \approx 10^{-7}$ kg/s, an initial pressure was $P_0 \approx 16$ torr $= 2130$ J/m^3 In the case $T_0 \approx 300$ K, the Xe-gas density is determined as $\rho_0 = P_0(\mu/k_B T_0) \approx 0.117$ kg/m^3 (particle density $n = 5\times10^{17}$ cm^{-3}), in which $\mu = 2.2\times10^{-25}$ kg is the mass of a Xe atom. The gas flow velocity in the tube 0 is $V_0 = G/S_0\rho_0 \approx 0.272$ m/s which is significantly smaller than the sound velocity $C_S = \sqrt{\gamma P_0/\rho_0} \approx 146$ m/s in the Xe gas, in which $\gamma = 5/3$ is the specific-heat-conduction ratio of the monatomic gas. When the gas flow transfers from the tube 0 to the orifice 1 while keeping G = const, the gas flow velocity increases as $V_1 = V_0/\alpha \approx 48$ m/s $\ll C_s$, which allows one to consider the gas flow through the orifice as a noncompressible cold gas (i.e., $\rho_0 \approx \rho_1$). According to the momentum conservation, $P_0 + \rho_0 V_0^2 = P_1 +$

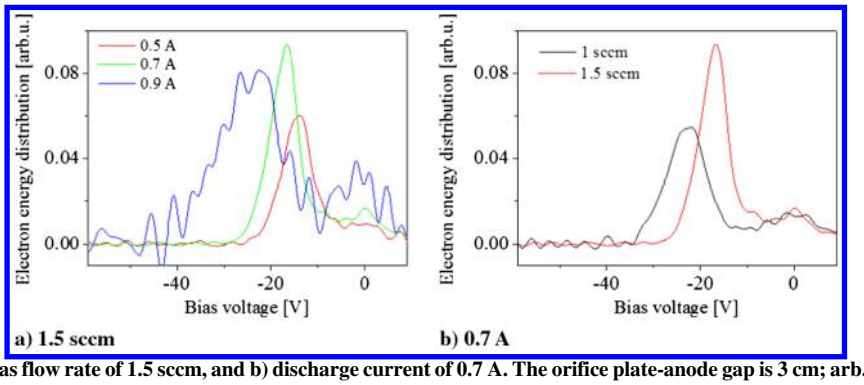

Fig. 13 EEDFs for a) Xe-gas flow rate of 1.5 sccm, and b) discharge current of 0.7 A. The orifice plate-anode gap is 3 cm; arb.u. denotes arbitrary units.

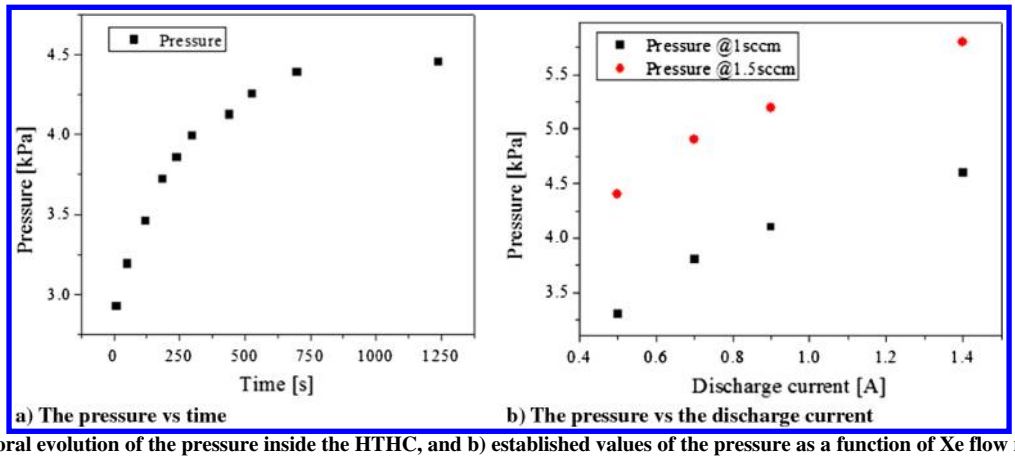

Fig. 14 a) Temporal evolution of the pressure inside the HTHC, and b) established values of the pressure as a function of Xe flow rate and discharge current.

$\rho_1 V_1^2$ and for $G = \text{const}$, the pressure decreases inside the orifice, $\Delta P = P_0 - P_1 \asymp \rho_1 V_1^2 = 274$ Pa. (here we neglected by $\rho_0 V_0^2 \ll P_0$).

In the case of the HTHC operation, to keep $G = \text{const}$, the value of the pressure in the tube 0 increases up to $P_0' = 3275$ J/m^3 However, the gas temperature in the tube 0 remains $T_0 \approx 300$ K that leads to the increase in the density and velocity of the gas, $\rho_0' = 0.202$ kg/m^3 and $V_0' = G/S_0\rho_0' \approx 28$ m/s $\ll C_S = \sqrt{\gamma P_0'/\rho_0'} \approx 178$ m/s, respectively. To estimate the gas temperature T_P inside the orifice, note that in the steady-state case, the velocity of the gas flow inside the orifice does not exceed the sound velocity. Using the momentum conservation, $P_0' = P_P + \rho_P C_P^2 = (1+\gamma)(kT_P\rho_P/\mu)$, in which the gas pressure is $P_P \approx (k/\mu)\rho_P T_P$, the sound velocity is $C_P = \sqrt{\gamma P_P/\rho_P}$, and the density is $\rho_P = G/S_{\text{or}}C_P$, one obtains

$$T_P \approx \frac{\gamma\mu}{k_B}\left(\frac{P_0' S_{\text{or}}}{G(1+\gamma)}\right)^2 \approx 1230 \text{ K}$$

This value of the gas temperature inside the orifice agrees satisfactorily with the value of the critical temperature estimated using Eq. (1), and is in good agreement with the emitter temperature estimated in [36]. For this temperature, the sound velocity is $C_P = \sqrt{\gamma k T_P/\mu} \approx 370$ m/s; the gas density is $\rho_P \approx 0.015$ kg/m^3, which results in total density of neutrals and ion $n \approx 6 \times 10^{16}$ cm^{-3}; and the pressure is $P_P \approx 1200$ Pa. Note here that this total ion and neutral density is smaller than the estimated density of electrons, $n_e \approx 1 \times 10^{17}$ cm^{-3} which one requires to carry a current of 0.5 A through the orifice. To explain this apparent contradiction, one can consider two explanations, namely, either the electron temperature is significantly larger than 1 eV, which was supposed in estimate of electron drift velocity, or there is a formation of a double layer in the vicinity of the orifice. The latter allows electrons to acquire a velocity sufficient to keep current continuity.

Without the HTHC operation (i.e., only cold Xe-gas flow), the density of the Xe gas flowing downstream toward the anode was measured using Penning probes at the distances from the exit of the orifice. The results of these measurements, shown in Fig. 15, revealed almost an exponential decrease in the neutral density vs the distance from the orifice exit and resulting in a density of Xe gas at the orifice exit of $\sim 5 \times 10^{17}$ cm^{-3} (pressure $\sim 2 \times 10^3$ Pa). This value of neutral density agrees well with the estimated cold-gas density, $n = 5 \times 10^{17}$ cm^{-3}.

F. Spectroscopic Measurements

First, the spectroscopic measurements were carried out using an open slit of the spectrometer with its grating placed at zero wavelength (i.e., without spectral resolution). These measurements showed that the HTHC operating in the diode mode results in a discharge, similar to a glow, forming between the cathode and the anode, and this discharge has a cone shape (see Fig. 7). It was found that the maximum of the continuous emission spectrum is shifted from red to blue with an increase in the discharge current from 0.4 to 1 A. The obtained shift of the plasma emission spectrum can be explained by the increase in the population of higher energy levels of excited Xe atoms, leading to the increase in the number of photons with larger energy emitted by electron spontaneous decay. The dominant mechanism of such excitations is electron impact collisions, and so electrons should increase their energy to excite atoms to higher energy levels. In fact, the energy spectrum of electrons consists of two maxima related to thermalized plasma electrons and an energetic (tens of electron volts) electron beam. Taking into account that the excitation energy of the obtained transitions is >8 eV, only a rather small part of the thermal electrons having a temperature of a few electron volts can participate in impact collisions leading to the excitation of electrons to these energy levels. Energetic electrons can effectively excite atoms (maximum cross section corresponds to $\sim 4E_{\text{ex}}$, in which E_{ex} is the excitation energy), and, indeed, a shift and broadening of the nonthermal EEDF with an increase in the discharge current (see Fig. 13a) have been observed, leading to a corresponding shift in the emission radiation spectrum. These energetic electrons also experience collisions with thermal-plasma electrons. The latter leads to the increase in the energy of these electrons, and, respectively, a larger part of the plasma electrons participates in the excitation of high energy levels. This indicates an increase in the electron temperature, allowing an increase in the density of neutrals excited to larger energy levels by electron impacts. Moreover, these space-resolved measurements showed that the discharge is characterized by the formation of a bright plasma spot in the vicinity of the orifice output. Typical frames of the spot dynamic obtained at different discharge currents are shown in Fig. 16.

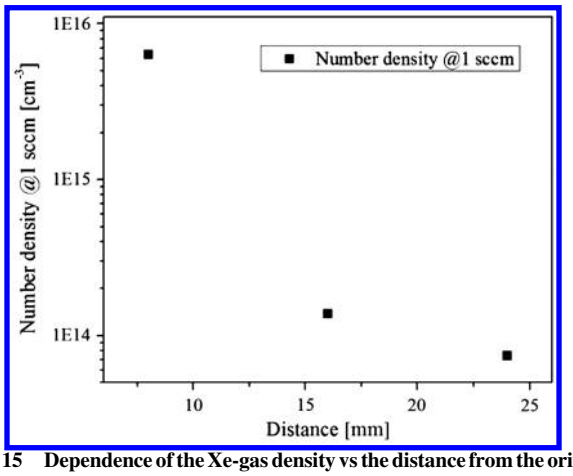

Fig. 15 Dependence of the Xe-gas density vs the distance from the orifice output along the cathode axis at a Xe-gas flow rate of 1 sccm.

It was found that the distance between the spot and the orifice output depends on the discharge current. The dependence of this distance and the spot emission spatial intensity along the symmetry axis on the discharge current is shown in Fig. 17. One can see that an increase in the value of I_d leads to an increase in the distance between the spot and the orifice output from ~0.1 mm at $I_d = 0.4$ A to ~0.7 mm at $I_d = 1$ A. In addition, a threefold increase in the value of I_d leads to an eightfold increase in the spot's intensity and significant (approximately fourfold) axial broadening of the spot.

Spectrally resolved measurements of the plasma spot showed that the plasma spectrum consists mainly of Xe II spectral lines and that there is no resolved spectral-line emission in the space between the orifice output and the plasma spot. One can suppose that electrons, which are extracted from the relatively cold plasma existing inside the orifice, are accelerated toward the anode, forming a dark space in the vicinity of the orifice output because the energy of these electrons is insufficient to produce excitation (Xe I excitation energy ≥ 8 eV and ionization energy ~12.1 eV) and ionization of Xe atoms. Thus, one can suppose that electrons gain energy equal to the ionization energy of Xe atoms at different distances depending on the discharge current (see Fig. 17a). The latter can be explained by the increase in the positive potential of the plasma existing inside the orifice with the increase in the value of the extracted electron current [30]. Note that the formation of the dense plasma spot does not influence the electric-field distribution due to the plasma polarization. This plasma serves as a source of relatively high-energy ion flux toward the emitter and the orifice plate, causing its erosion. Thus, electrons emitted from the boundary of the plasma at the exit of the orifice will gain energy sufficient for the ionization and excitation of Xe gas at larger distances from the orifice output (see Fig. 17a). An effective ionization of Xe neutrals in the orifice vicinity (location of the plasma spot) leads to the formation of relatively dense plasma, an increase in electron collisionality, and, respectively, an increase in electron-energy losses. An increase in the value of I_d leads to an increase in the density and temperature of this plasma that qualitatively agrees with the results of the intensity's dependence on I_d shown in Fig. 17b. Here, note that the neutral density (see Fig. 15) in the few millimeters from the orifice exit is ~6×10^{15} cm^{-3}, which dictates the mean free path of several hundreds of microns for electrons, with energy sufficient for ionization and excitation. Thus, almost all the electrons that are emitted from the plasma located at the orifice exit lose their energy ionizing neutrals and experience thermalization, forming a dense plasma spot that becomes the source of electrons accelerated toward the anode.

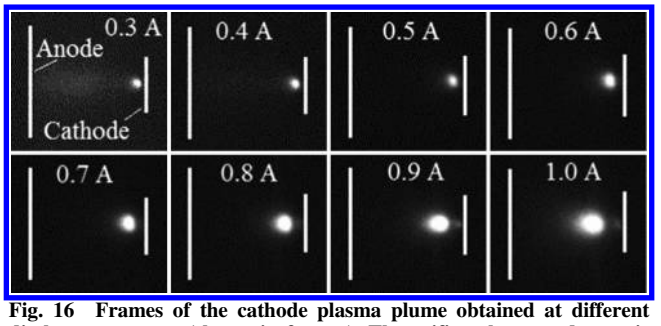

Fig. 16 Frames of the cathode plasma plume obtained at different discharge currents (shown in frames). The orifice plate–anode gap is 3 cm; the Xe-gas flow rate is 1 sccm.

The plasma spot emits enough light to allow spectroscopic measurements, and this spot has small spatial variations along the line of sight. Thus, reliable and reproducible measurements of the plasma density and temperature become possible. In many cases, it is necessary to distinguish between the electron, ion, and atom temperatures, which may differ significantly from each other. Here, due to higher electron–electron collision rates, it is assumed that the electron-velocity distribution is close to Maxwellian. It was found that the emission spectrum of the plasma spot consists of several strong spectral lines of Xe II ions, namely, 484.433, 529.222, 460.303, 541.915, and 597.646 nm. Two of these spectral lines [i.e., 460.303 nm (transition 14.48–11.79 eV) and 541.915 nm (transition 14.07–11.79 eV)], having the same low energy level of the transition, were chosen to estimate the ratio of the population density of the upper energy levels. This ratio is determined by the value of Einstein coefficients for spontaneous emission of these transitions and by the branching ratio of these transitions to other transitions from these upper energy levels. The selected spectral lines can be considered as isolated, which allows the full spectral image of the plasma spot to be recorded with the open entrance slit of the spectrograph and using the camera's charge-coupled-device pixels (8.6×8.6 μm) for spatial-resolution determination. The plasma spot was scanned using an axial step of 150 μm with a spatial resolution of 70 μm for two values of discharge current, 0.7 and 0.9 A. In the case of a Boltzmann distribution of energy-level population, the ratio of two spectral lines can be used to obtain the plasma electron temperature as

$$kT_e = \frac{E_{u_2} - E_{u_1}}{\ln\left(k_{\text{system}} \frac{I_{\text{ul}}^{1\text{observed}}}{I_{\text{ul}}^{2\text{observed}}} \cdot \frac{g_{u_2} A_{u_2 l_2} \nu_{u_2 l_2}}{g_{u_1} A_{u_1 l_1} \nu_{u_1 l_1}}\right)}$$

in which g_u and g_l are the degeneracy; E_u and E_l are the energies of the upper and low energy levels u and l, correspondingly; A_{ul} is the spontaneous-emission coefficient; ν_{ul} is the transition frequency of these transitions; k is the Boltzmann constant; k_{system} is the optical-system sensitivity coefficient obtained using a calibrated blackbody lamp; and $I_{\text{ul}}^{1\text{observed}}$ and $I_{\text{ul}}^{2\text{observed}}$ are the intensities of the spectral lines.

The dependencies of the population ratio $\delta = (n_{E^{14.47\text{ eV}}}/n_{E^{14.07\text{ eV}}})$ on the distance within the plasma spot are shown in Fig. 18 for two values of I_d. One can see that this ratio decreases monotonically toward the anode, indicating a decrease in the electron temperature, assuming Boltzmann distribution of these high-energy-level populations. Moreover, at a certain distance (depending on the discharge current), this ratio exceeds 1, which corresponds to a negative value of T_e. The latter strongly indicates that the Boltzmann distribution of level population does not existed at the spot areas

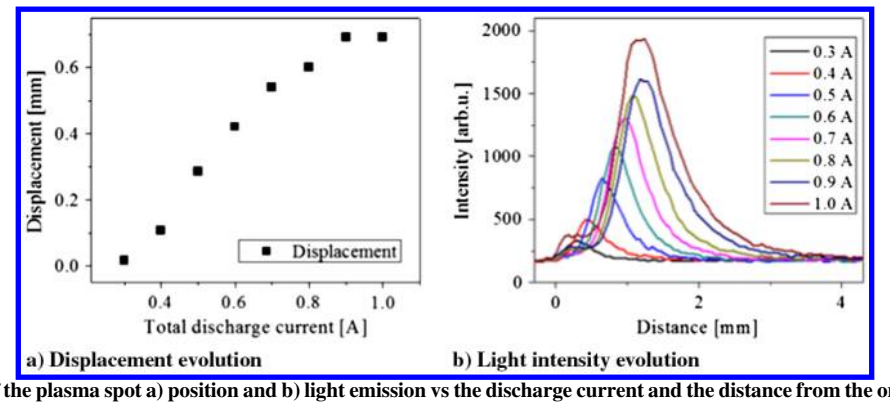

Fig. 17 Dependencies of the plasma spot a) position and b) light emission vs the discharge current and the distance from the orifice output, respectively.

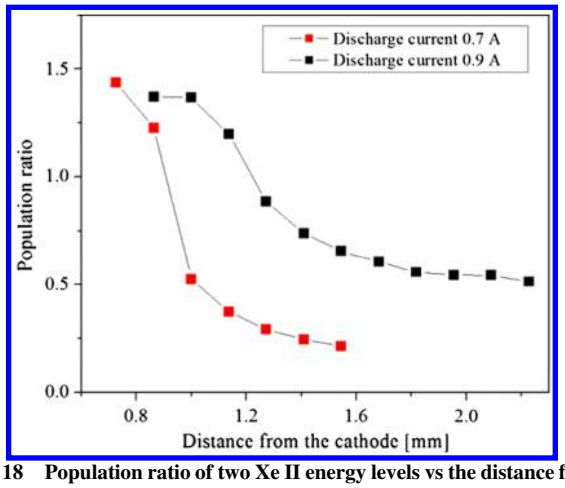

Fig. 18 Population ratio of two Xe II energy levels vs the distance from the orifice output. The orifice plate-anode gap is 3 cm; the Xe-gas flow rate is 1 sccm.

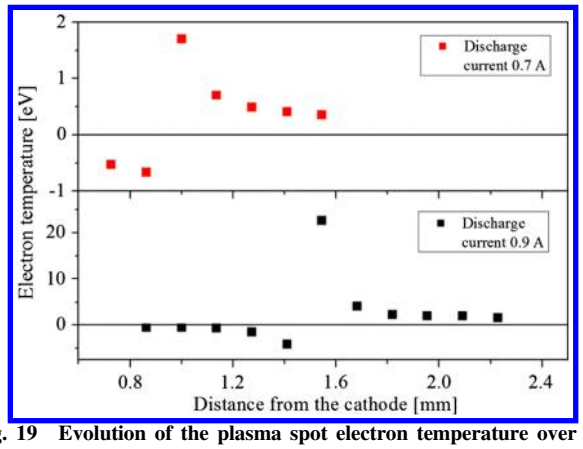

Fig. 19 Evolution of the plasma spot electron temperature over the plasma plume. The Xe-gas flow rate is 1 sccm and the orifice plate–anode gap is 3 cm.

closest to the orifice plasma. The dependencies of the plasma electron temperature (assuming Boltzmann distribution of level population) inside the plasma-spot plume on the distance from the orifice output for two values of the discharge current are shown in Fig. 19. One can suppose that in locations with negative temperature, electrons extracted from the orifice plasma boundary obtain an energy spectrum that allows the excitation of the upper levels of Xe II first, leaving the underlying energy levels less populated [31]. Because of the high ionization rate in this region, a dense plasma is formed and electrons are effectively thermalized by collisions, reaching equilibrium-energy distribution within hundreds of microns. At these distances, the plasma electron temperature was estimated to be in the range of a few electron volts with a larger electron temperature for larger values of the discharge current (see Fig. 19).

Finally, the absolute calibration of the optical setup using a calibrated standard irradiance lamp (SN7-1732) allows the authors to obtain the plasma density as $n = n_i Z(T_e)/[g_i \exp(-E_i/kT_e)$, in which $n_i = k_{\text{system}} I^{\text{observed}}/(A_i h\nu_i)$ is the ion excited-level population density, T_e is the known plasma electron temperature, and $Z(T_e) = \sum_i g_i \exp[-(Ei)/(kTe)]$ is the partition function. For absolute calibration of the spectroscopic system, the black screen with a small central hole was installed perpendicular to the spectroscopic axes intersecting the cylindrical axes of the cathode. The space resolution and field of view of the spectroscopic system were determined by a straight observation of a metric ruler through a given entrance-slit width of the spectrograph at zero grating position. The standard spectral-irradiance lamp was installed on the spectroscopic axes 0.5 m behind the screen, providing a known photon flux (manufacturer's calibration report) through the hole in the screen. This photon flux was recorded at different wavelengths by an intensified charge-coupled-device (ICCD) camera attached to the spectrograph, allowing the authors to calculate the system coefficient k_{system} mentioned previously. The exposure time of the camera was adjusted to obtain similar intensities (i.e., amount of photons) during the calibration procedure and experiment to avoid a possible nonlinear response of the spectroscopic system [mostly caused by the microchannel plate (MCP) module of the ICCD camera] on the photon flux, whereas the gain was kept the same. The linearity of the spectral-line intensity vs the exposure time at a given MCP gain (up to 100 μs) was carefully checked by measurements.

The spatial distribution of the plasma-spot density inside the orifice plate–anode gap is shown in Fig. 20. It can be seen that there is a sharp increase in plasma density up to 10^{16} cm^{-3} at a few millimeters from the orifice plate of the cathode, which agrees with the data presented in Fig. 17b; the plasma density monotonically decreases toward the anode. Note that the maximum value of the plasma-spot density exceeds the plasma-plume density by almost six orders of magnitude.

IV. Conclusions

It was found that the heaterless thermionic hollow cathode (HTHC) ignition consists of a sequence of emitter–orifice (EO)-

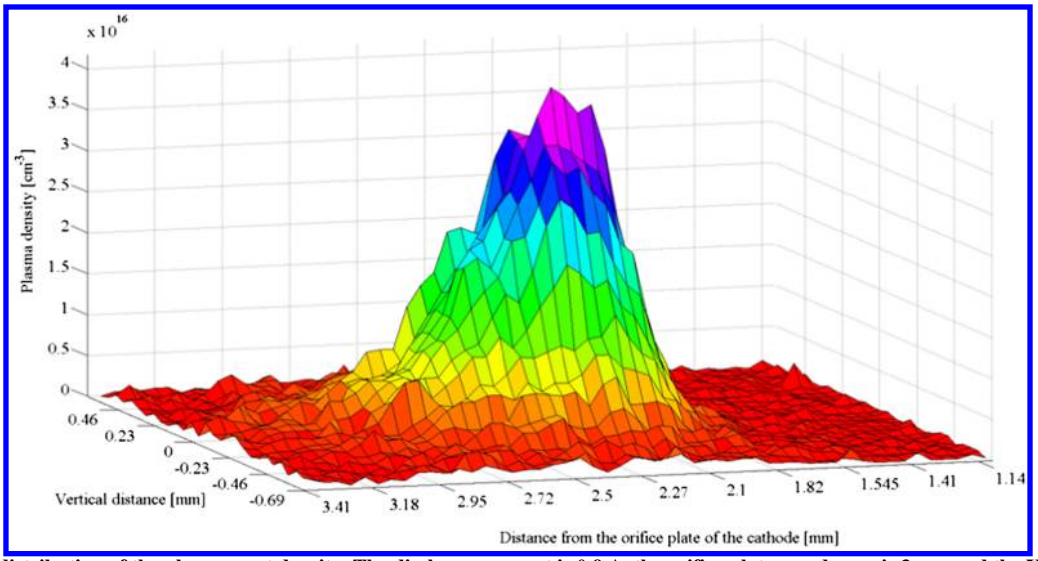

Fig. 20 Spatial distribution of the plasma-spot density. The discharge current is 0.9 A, the orifice plate–anode gap is 3 cm, and the Xe-gas flow rate is 1 sccm.

plate-gap breakdown, emitter heating, and its temperature maintenance (keeping), and can be realized without any additional external heater within the millisecond timescale with a power consumption of less than 30 W. A reliable main-discharge ignition between the emitter and the anode can be achieved in the final keeping phase of the emitter heating when the potential distribution between the emitter, orifice, and anode allows electrons to reach the anode.

It was shown that to achieve this reliable HTHC ignition, the length of the EO-plate gap and xenon (Xe)-gas flow rates should be adjusted to satisfy optimal conditions, namely, to allow a low voltage breakdown (the first phase), an effective and fast heating of the emitter (the second phase), and the capability to ignite and sustain the main discharge (the third phase). A proper realization of these conditions can extend the lifetime of the heaterless hollow cathode to that of conventional cathodes retaining the main advantages of the heaterless design.

During the main discharge, the HTHC emitter should be at a certain temperature to provide the required discharge current. Any change in the extracted current amplitude leads to self-consistent adjusting of the plasma parameters inside the emitter. The discharge established between the orifice plate and the anode can be considered as a glow discharge. This discharge is characterized by a dark space, where the electrons gain energy sufficient for gas ionization and excitation, and a region of bright-light-emission plasma where Xe-gas atoms are ionized by the extracted electron beam. It is supposed that this dense plasma with a density of $\sim 10^{16}$ cm^{-3} and an electron temperature of a few electron volts can be considered as a source of electrons that are accelerated toward the anode. These electrons produce ionization of the Xe gas inside the remaining orifice plate–anode gap, forming a dilute plasma with density and temperature in the ranges $((10^9–10^{10})\text{cm}^{-3}$ and (1–2.5)eV, respectively. Measurements of electron-energy distribution function revealed that electrons gain an energy of 20–30 eV (depending on the discharge current and Xe flow rate), probably in the gap between the plasma-plume spot–anode, forming the electron beam.

Acknowledgments

The authors wish to thank Andrey Loyan for fruitful discussions and comments, and Andrey Levin and Kalman Gruzinsky for generous technical assistance.

References

[1] Benford, J., and Swegle, J., *High-Power Microwaves*, Artech House, London, 1992, pp. 148–156.

[2] Granatstein, V., and Alexeff, I., *High Power Microwave Sources*, Artech House, Boston, 1987.

[3] Bakish, R., and White, S. S., *Handbook of Electron Beam Welding*, Wiley, New York, 1964.

[4] Liu, S., Dougal, R. A., and Lyons, J. S., "Heat Treatment of Metal Surfaces by a Conformal Electron Beam," *Journal of Engineering Materials and Technology*, Vol. 123, No. 2, 2001, pp. 210–215. doi: 10.1115/1.1338480

[5] Goebel, D., and Katz, I., *Fundamentals of Electric Propulsion: Ion and Hall Thrusters*, Wiley, Hoboken, NJ, 2008, pp. 243–315.

[6] Dushman, S., "Electron Emission from Metals as a Function of Temperature," *Physical Review*, Vol. 21, No. 6, 1923, pp. 623–636. doi: 10.1103/PhysRev.21.623

[7] Fowler, R., and Nordheim, L., "Electron Emission in Intense Electric Fields," *Proceedings of the Royal Society of London, Series A: Mathematical and Physical Sciences*, Vol. 119, No. 781, 1928, pp. 173–181. doi: 10.1098/rspa.1928.0091

[8] Micci, M., and Ketsdever, A. (eds.), *Micropropulsion for Small Spacecraft*, Vol. 187, Progress in Astronautics and Aeronautics, AIAA, Reston, VA, 2000, pp. 45–84.

[9] Long, K. F., *Deep Space Propulsion: A Roadmap to Interstellar Flight*, Springer, New York, 2011, pp. 139–153.

[10] Bridges, W. B."Ionized Gas Lasers," in *Handbook of Laser Science and Technology Vol. II: Gas Lasers*, CRC Press, Boca Raton, FL, 1982, p. 171.

[11] Mesyats, G., Osipov, V., and Tarasenko, V., *Pulsed Gas Laser*, SPIE Press, Bellingham, WA, 1995, pp. 1–19.

[12] Gold, S., and Nusinovich, G., "Review of High-Power Microwave Source Research," *Review of Scientific Instruments*, Vol. 68, No. 11, 1997, pp. 3945–3974. doi: 10.1063/1.1148382

[13] Oks, E., *Plasma Cathode Electron Sources: Physics, Technology, Applications*, Wiley-VCH, Berlin, 2006, pp. 2–6, 59–75.

[14] Krasik, Ya. E., Yarmolich, D., Gleizer, J. Z., Vekselman, V., Hadas, Y., Gurovich, V. Tz., and Felsteiner, J., "Pulsed Plasma Electron Sources," *Physics of Plasmas*, Vol. 16, No. 5, 2009. doi: 10.1063/1.3085797

[15] Jahn, R., and Choueiri, E., "Electric Propulsion," *Encyclopedia of Physical Science and Technology*, 3rd ed., edited by Myers, R. A., Vol. 5, Academic Press, San Diego, CA, 2002, pp. 125–141.

[16] Patterson, M., Domonkos, M., Carpenter, C., and Kovaleski, S., "Recent Development Activities in Hollow Cathode Technology," IEPC 01-270, Oct. 2001.

[17] Rubin, B., and Williams, J., "Hollow Cathode Conditioning and Discharge Initiation," *Journal of Applied Physics*, Vol. 104, No. 5, 2008, pp. 2–6. doi: 10.1063/1.2973690

[18] Schatz, M., "Heaterless Ignition of Inert Gas Ion Thruster Hollow Cathodes," NASA, Lewis Research Center, Cleveland, Ohio, 1985.

[19] Arkhipov, B., "Development and Research of Heaterless Cathode Neutralizer for Linear Hall Thruster (LHD) and Plasma Ion Thrusters (PIT)," *Proceedings of the 25th International Electric Propulsion Conference*, Cleveland, OH, 24–28 Aug. 1997; also IEPC 97-175.

[20] Sarver-Verhey, T., and Hamley, J., "Discharge Ignition Behavior of the Space Station Plasma Contactor," *30th Joint Propulsion Conference AIAA*, Indianapolis, Indiana, June 1994.

[21] Domonkos, M., Gallimore, A., Williams, G., and Patterson, M., "Low-current Hollow Cathode Evaluation," *35th Joint Propulsion Conference*, Los Angeles, CA, June 1999; also AIAA 99-2575.

[22] Koroteev, A., Pelrosov, V., Baranov, V., and Vasin, A., "Development of 4 kW Hall-type Electric Thruster," *International Electric Propulsion Conference*, Los Angeles, CA, Sept. 1993; also IEPC 93-225.

[23] Koshelev, N., and Loyan, A., "Investigation of Hollow Cathode for Low Power Hall Effect Thruster," IEPC 2007-103, Sept. 2007.

[24] Loyan, A. V., Koshelev, N. N., Solonynko, Ye. P., and Ageeva, E. G., "Preliminary Testing of W-Ba-Sc Emitters of EPT Cathodes," *Journal of Aerospace Engineering & Technology*, Vol. 8, No. 75, 2010, pp. 68–72 (in Russian).

[25] Mott-Smith, H. Jr., and Langmuir, I., "The Theory of Collectors in Gaseous Discharges," *Physical Review*, Vol. 28, No. 4, 1926, p. 727. doi: 10.1103/PhysRev.28.727

[26] Godyak, V. A., and Demidov, V. I., "Probe Measurements of Electron-Energy Distributions in Plasmas: What Can We Measure and How Can We Achieve Reliable Results?," *Journal of Physics D: Applied Physics*, Vol. 44, No. 23, 2011, pp. 4–10. doi: 10.1088/0022-3727/44/23/233001

[27] Pashchen, F., "Ueber die zum Funkenübergang in Luft, Wasserstoff und Kohlensäure," *Annalen der Physik*, Vol. 273, No. 5, 1889, pp. 69–96. doi: 10.1002/andp.18892730505

[28] Kruithof, A., "Townsend's ionization coefficients for neon, argon, krypton and xenon," *Physica*, Vol. 7, No. 6, June 1940, pp. 519–540. doi: 10.1016/S0031-8914(40)90043-X

[29] Vekselman, V., Gleizer, J. Z., Yatom, S., Gurovich, V. Tz., and Krasik, Ya. E., "High-Current Diode with Ferroelectric Plasma Source-Assisted Hollow Anode," *Journal of Applied Physics*, Vol. 108, No. 9, 2010, pp. 6–7. doi:10.1063/1.3486450

[30] Raizer, Y. P., *Gas Discharge Physics*, Springer, Berlin, 1991, pp. 103–123.

[31] Goebel, D., Jameson, K., Witkins, R., and Katz, I., "Hollow Cathode and Keeper-Region Plasma Measurements Using Ultra-Fast Miniature Scanning Probes," AIAA Paper 2004-3430, July 2004.

[32] Jameson, K., Goebel, D., and Watkins, R., "Hollow Cathode and Keeper Region Plasma Measurements," AIAA Paper 2005-3667, July 2005.

[33] Williams, J., and Wilbur, P., "Electron Emission from a Hollow Cathode-Based Plasma Contractor," *Journal of Spacecraft and Rockets*, Vol. 29, No. 6, 1992, pp. 820–829. doi:10.2514/3.25537

[34] Hershcovithch, A., "High-Pressure Arcs as Vacuum-Atmosphere Interface and Plasma Lens for Nonvacuum Electron Beam Welding Machines, Electron Beam Melting, and Nonvacuum Ion Material Modification," *Journal of Applied Physics*, Vol. 78, No. 9, 1995,

pp. 5283–5288.
doi: 10.1063/1.359704

[35] Krasik, Ya. E., Gleizer, S., Gurovich, V., Kronhaus, I., Hershcovithch, A., Nozar, P., and Taliani, C., "Plasma Window Characterization," *Journal of Applied Physics*, Vol. 101, No. 5, 2007, pp. 053305-1–053305-5.
doi:10.1063/1.2472280.

[36] Domonkos, M., Gallimore, A., Williams, J., and Patterson, M., "Low Current Hollow Cathode Evaluation," AIAA Paper 99-2575, June 1999.

L. King
Associate Editor